

On the Use of CVRP to Diagnose Faulty Elements in Antenna Arrays

Alejandro Antón Ruiz*, John Kvarnstrand†, Klas Arvidsson†, Andrés Alayón Glazunov*‡

*University of Twente, Enschede, The Netherlands, {a.antonruiz a.alayonglazunov}@utwente.nl

†Bluetest AB, Gothenburg, Sweden, name.familyname@bluetest.se

‡Linköping University, Norrköping Campus, Sweden, andres.alayon.glazunov@liu.se

Abstract—This paper investigates the application of Constrained-View Radiated Power (CVRP) for diagnosing phased array element failures, specifically focusing on on-off element failure. CVRP, similar to Partial Radiated Power (PRP), considers a specific Field-of-View (FoV) but normalizes it by the FoV area. The study explores CVRP's effectiveness in detecting failures in a 2x8 cosine element array under beam-steering conditions, accounting for random and depointing errors, angular resolution, and pattern rotation. Results indicate that CVRP can detect on-off failures based on angular resolution and error severity, under the assumption of reduced Total Radiated Power (TRP) with element failures. Additionally, CVRP is effective with partial far-field patterns, making it suitable for near-field, indirect far-field, and far-field measurement systems without requiring phase acquisition in the latter two.

Index Terms—Phased Array, Array Failure, Diagnostics, Antenna Measurements.

I. INTRODUCTION

With the increasing use of Millimeter Wave (mmWave) systems for radar, Fifth Generation (5G), and satellite communications [1], more array antennas are being produced. Such antennas are ideal to compensate for the increased pathloss at mmWave and, due to their directive nature, it is necessary that they can be focused where it is needed. Phased arrays enable this feature by applying beamsteering through phase, amplitude, or both, excitation of their elements.

Testing of phased arrays generally belongs to Over-The-Air (OTA) testing, since their antenna feed ports cannot generally be accessed [2]. Testing is an essential step in product development and production. In particular, OTA testing provides a performance evaluation of the whole wireless device, phased array in this case in a controlled environment, which offers comparability between, e.g. multiple production units.

One relevant outcome of OTA testing is the Equivalent Isotropic Radiated Power (EIRP) radiation pattern. It can be obtained either from direct or indirect far-field systems, as well as near-field ones. OTA testing has an added layer of complexity for near-field systems since phase acquisition is needed and phase synchronization of the measurement instrument with the Device Under Test (DUT) is generally not possible, so it is needed to resort to phase recovery techniques [3].

A Figure of Merit (FoM) is commonly used to condense information acquired from measurements. In the case of the EIRP radiation pattern, there are several FoMs of interest to

characterize the performance of the DUT. They can be point quantities, such as maximum EIRP, integral quantities, such as Total Radiated Power (TRP), or partial integral quantities, such as Partial Radiated Power (PRP) [4], and Constrained-View Radiated Power (CVRP), introduced in [5]. The latter FoMs, by their partial integral nature, can be used as FoMs to characterize the quality of the coverage of the DUT, i.e., how successful the DUT is in focusing the transmitted power into a coverage area. However, it was shown in [5] the application of CVRP to detect faulty elements in an antenna array. One main advantage of using this partial quantity is eliminates the need to acquire the full pattern. Moreover, since CVRP is based solely on EIRP values, it remains applicable across any measurement range, whether in direct far-field, indirect far-field, or near-field scenarios.

In this work, we further investigate the feasibility of using CVRP to determine if an antenna array has a certain amount of faulty elements, which was preliminary presented in [5], where it was applied to experimental results. There are several methods to diagnose faulty elements on an array. Some of them make use of the phase information of the radiation pattern to solve an inverse problem and retrieve the excitation coefficients [6], [7], [8]. There are other methods, which include the use of machine learning, that use amplitude-only data from the far-field pattern [9], [10], while others make use also of the phase information [11]. To the best of the authors' knowledge, there is not a thorough investigation on methods to detect failed array elements using far-field amplitude-only data without the need to resort to machine learning approaches, which require a complex process to be trained and validated.

In this study, we consider a 2 by 8 ideal cosine elements array, and take into account the following factors:

- On-off faulty elements: elements are turned completely off. Coupling is not considered.
- Beamsteering
- Effect of pattern rotation needed when beamsteering is applied
- Angular resolution
- Systematic (depointing) errors
- Random (ripple) errors

II. CVRP AND ITS APPLICATION

CVRP was introduced in [5], so we just show the equation of the approximation used when we have a EIRP radiation

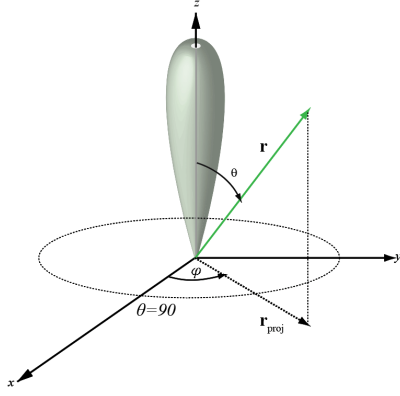


Fig. 1. Definition of φ and θ . Source: [12].

pattern over a discretized θ and φ grid and the particular application used in this paper

$$CVRP \cong \frac{\Delta\varphi\Delta\theta}{A} \sum_{i=1}^{N-1} \sum_{j=0}^{M-1} EIRP_{Total,msk}(\theta_i, \varphi_j) \sin(\theta_i), \quad (1)$$

where $EIRP_{Total,msk}(\theta_i, \varphi_j)$ is the sum of the EIRP in two orthogonal polarizations in linear scale (e.g. mW), masked by the considered $[-\frac{\varphi_{FoV}}{2}, \frac{\varphi_{FoV}}{2}]$ and $[0, \theta_{FoV}]$. In particular, the values of $EIRP_{Total,msk}(\theta_i, \varphi_j)$ are set to 0 for any θ_i, φ_j outside of the considered intervals. A is the area of the (partial) sphere defined by the considered φ and θ intervals. $\Delta\varphi$ and $\Delta\theta$ are the grid step sizes or angular resolutions, in radians, defining the number of sampling points for φ , $M = \frac{2\pi}{\Delta\varphi}$, and for θ , $N = \frac{\pi}{\Delta\theta}$.

Throughout this work, we always consider a φ_{FoV} of 360° , varying θ_{FoV} . Please note that we use the definitions of φ and θ shown in Fig. 1. For the limiting case where $\theta_{FoV} = 0^\circ$, we make $CVRP = EIRP_{Total}(0, 0)$, which is the EIRP corresponding to the positive z-axis. For the other limiting case, where $\theta_{FoV} = 180^\circ$, the CVRP equals the TRP, being $A = 4\pi$, which is the area of the unit sphere.

The result of CVRP can be interpreted as the TRP that an ideal isotropic radiator would need to have to provide the same CVRP over the considered area, which can be used to evaluate the power focusing in the considered area. The main difference with PRP is the normalization by only the considered area and not the whole sphere. This enables the comparison of CVRP values at different considered areas, defined in our case by θ_{FoV} . This can be easily understood with the example of an ideal isotropic radiator, where the CVRP would be constant over all θ_{FoV} values and equal to its TRP, while the PRP will be larger with an increasing considered area, until reaching the TRP when considering the full sphere.

One of the consequences of defining the CVRP centered in the positive z-axis is that, whenever we have an antenna whose main lobe is not aligned with the positive z-axis, e.g. when we apply beamsteering, to perform an adequate comparison in terms of CVRP with the broadside case we need to rotate the EIRP radiation pattern so that the main lobe is aligned with the z-axis, which implies an interpolation of the original

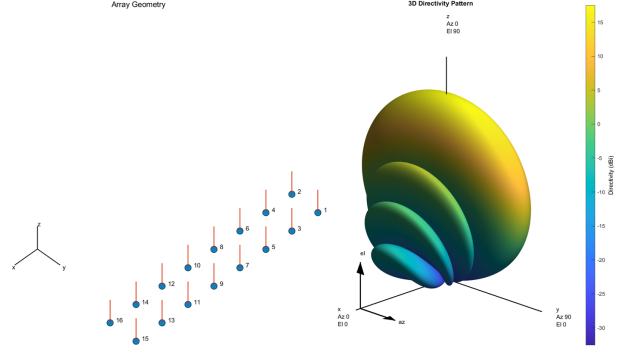


Fig. 2. Simulated array geometry and directivity pattern. On the left, the array geometry plot includes the indexes of each element, as well as their normals in red. Generated using the Sensor Array Analyzer app from MATLAB.

values. In this work, only linear interpolation of the radiation pattern EIRP linear values is considered.

III. SIMULATION SETUP

A. Antenna array

The antenna array considered for this work is a 2 by 8 ideal cosine elements array, with 0.5λ spacing in both dimensions. The frequency of operation is 28 GHz, but, due to the wavelength-dependent layout of the array and the idealized elements, the results are independent of the considered frequency. Its normal in its unmodified state is aligned with the z-axis. The array layout and base radiation pattern can be observed in Fig. 2. The elements used are the cosine ones, located under the antenna section, with a cosine power of $[1, 1]$.

B. Faulty elements

This work only considers on-off element failures, which implies that the weighting of the failed element is set to 0. Since we have the radiation pattern in terms of directivity, we convert it to EIRP by summing a TRP value. For similarity to [5], we choose the base value to be $TRP_{base} = 15$ dBm. Unlike what was observed in [5], where deactivating array elements did not seem to impact the outputted TRP, we consider here that the outputted TRP is reduced proportionally to the number of failed elements. In particular, we have that

$$TRP \text{ [dBm]} = TRP_{base} + 10 \log_{10} \frac{N_{el} - N_{FE}}{N_{el}}, \quad (2)$$

where $N_{el} = 16$ is the number of array elements, N_{FE} is the number of failed elements, and There are 4 considered cases in terms of element failures, denoted as “FE X”, where “X” represents the failed elements. If “X” is 0 it means that no elements fail. The indexes of the array elements can be observed in Fig. 2:

- FE 0: $TRP = 15$ dBm
- FE 15: $TRP = 14.72$ dBm
- FE 7 9: $TRP = 14.42$ dBm
- FE 7 8 9 10: $TRP = 13.75$ dBm

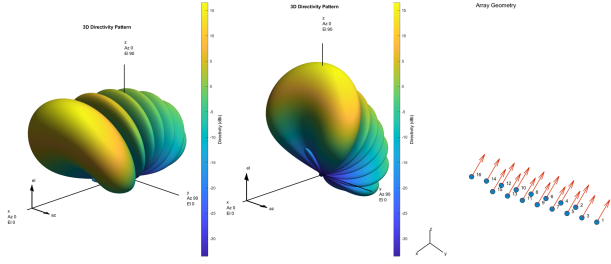


Fig. 3. Simulated array geometry and directivity pattern. On the left, the pattern of the array with 45° beamsteering without rotation. In the middle, the pattern of the array with 45° beamsteering and a 45° clockwise rotation around the y-axis. On the right, the geometry of the array with the 45° clockwise rotation around the y-axis. Note that the rotation is applied to both the positions of the elements and their normals. Also, note that the geometry of the array without the rotation is the same as the one depicted in Fig. 2.

C. Beamsteering

Two cases of beamsteering are considered in this work. The first is not applying any beamsteering, i.e., what can be observed in Fig. 2. The other case is a 45° steering from the positive z-axis and towards the positive x-axis, contained in the xz plane, so the main beam is pointing towards $\theta = 45^\circ$ and $\varphi = 180^\circ$ in the coordinate system from Fig. 1. As stated in the end of Section II, we need to rotate this radiation pattern to align the main lobe with the positive z-axis. This is done by applying a 45° clockwise rotation around the y-axis to the radiation pattern. Without going into further detail, we just want to highlight that this implies an interpolation (linear, in this case) of the values of the original radiation pattern. Therefore, we are introducing an error. To evaluate the impact of this introduced error, we rotate the array 45° clockwise around the y-axis, so that we have an error-free version of the pattern with the main lobe aligned with the positive z-axis to compare with the version rotated in post-processing. This is relevant since it allows us to evaluate the impact of the post-processing rotation, which will most likely be performed when taking actual measurements, as was the case in [5]. We will refer to this rotation of the array before acquiring the radiation pattern as “physical rotation”, in contrast with the “post-processing rotation”. All this can be better understood with Fig. 3. We will denote this variable as “SA”.

D. Angular resolution

This study considers three different angular resolutions: 0.5°, 1.5° and 5°. We consider 19 unique values of θ_{FoV} , ranging from 0° (where the CVRP equals the EIRP of the positive z-axis, after any possible rotation), to 180° (where the CVRP equals the TRP), with a 10° step size. We will denote the angular resolution variable as “RES”.

E. Depointing errors

These systematic errors emulate the misalignment between the DUT’s broadside and the measurement antenna that might occur in a real testing setup. They are applied by applying a “physical rotation” to the array elements and their normals. We consider depointing errors of 1° and 3°, both of them in

a clockwise fashion around the y-axis. We will denote this variable as “DEP”.

F. Random errors

We consider random errors on the acquisition of the radiation pattern. In particular, we aim to emulate a ripple error that could occur when using a Compact Antenna Test Range (CATR) system. We base our error model in [13], [14], [15]. We consider a ripple error $\sigma_{err,dB}$ of 1 and 2 dB. As stated in [13], we have that $\sigma_{err,lin} = 23 \cdot \sigma_{err,dB}/100$. Then, we apply

$$EIRP_{Total,err}(\theta_i, \varphi_j) = EIRP_{Total}(\theta_i, \varphi_j) \cdot (1 + \mathcal{N}(0, \sigma_{err,lin}^2)), \quad (3)$$

so every point of the radiation pattern gets distorted by a random amount which is proportional to its original value, thus obtaining a distorted radiation pattern. The objective of simulating this error is to obtain a confidence interval of the CVRP values for each θ_{FoV} and for every combination of the rest of the factors. This is attained by obtaining CVRP values for 1000 different distorted patterns for each $\sigma_{err,dB}$ value. Then, we estimate the standard deviation of each CVRP value from the 1000 acquired values ($\hat{\sigma}_{lin}$), and compute the 95% Confidence Interval (CI) as

$$CVRP [mW] = \text{mean}(CVRP_{sim}) \pm 1.962 \cdot \hat{\sigma}_{lin}, \quad (4)$$

where 1.962 comes from the t-score for 95% confidence and 999 degrees of freedom.

IV. RESULTS

In this section, we present the results of the simulations described in Section III. We divide the results considering several factors at a time or separately. In general, we present the results as the subtraction of the result of interest and a reference value, with the objective to see if it is possible to discern between each case. Note that the ultimate goal is to find out if, considering all introduced errors, it is possible, and if so, in which cases, to distinguish the number of failed elements between the 4 different cases.

A. Effect of post-processing rotation

First, we show the impact of the post-processing rotation of the pattern in the CVRP values by comparing them to the physical rotation ones. This quantifies the error introduced by the post-processing rotation that is needed when we perform beamsteering. In Fig. 4, it can be observed that, for the finest angular resolution of 0.5°, the introduced error is lower than 0.015 dB in all cases (note that the red line is behind the dark blue line), so we can consider it negligible. For the coarsest angular resolution of 5°, the introduced error reaches a maximum of around 0.15 dB, with a rapid oscillation for values of θ_{FoV} between 10° and 20°, although it is drastically reduced when considering larger θ_{FoV} , going lower than 0.08 dB. We can also observe that the error is generally higher when more than one element fails, probably due to the increased irregularities of the radiation pattern, that degrade the linear interpolation accuracy. It is also worth noting that the effect for $\theta_{FoV} = 0^\circ$ is negligible in all cases.

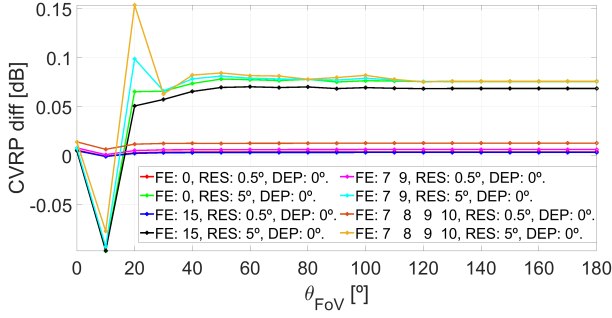


Fig. 4. Post-processing rotation CVRP minus physical rotation CVRP for 45° beamsteering case. The same angular resolution (“RES”) is used for computing the CVRP values to be subtracted, e.g., the case “FE: 15, RES: 5°, DEP: 0°” is the result of the case “FE: 15, RES: 5°, DEP: 0°” with post-processing rotation minus the case “FE: 15, RES: 5°, DEP: 0°” with physical rotation. No depointing nor random errors are considered.

B. Effect of all errors

We have discussed the impact of the post-processing rotation in Section IV-A. However, in a realistic scenario, we would not acquire a measurement where we physically rotate the DUT, since it might not be mechanically feasible, or, moreover, it could increase the uncertainty of the measurement due to a change in the position of the DUT from one measurement to another.

Therefore, we now consider that we measure without any physical rotation, other than the depointing cases. We also consider that we are unaware of the depointing and that we do not correct for it by doing a post-processing rotation to revert it. This might be something obvious to do when we have all elements without failure, since it would be just a matter of searching maximum EIRP and then rotating the pattern so that point is aligned with the positive z-axis. However, when we have failure in some elements, the maximum EIRP is generally no longer in the intended scanning direction.

As reference measurements, we will take the cases without any failed elements, with the corresponding angular resolution, and without any depointing. We do this because we consider that it would be a common practice to test the “golden device”, i.e., one that we know by other means that has no failed elements with the same resolution that will be used to measure the DUTs to test and we also consider that it would be reasonable to assume that a calibration of the alignment is performed for the measurement of the “golden device”, but not necessarily for the other DUTs. We show the results that we consider that provide the most relevant information, i.e. the worst-case scenarios.

With this into account, we can observe Fig. 5 and Fig. 6, where we can see the traces for 4 cases combining the number of faulty elements and depointing. It is worth noting that, to distinguish if we have, in this case, 1 failed element (number 15) or no failed elements with at least a 95% of confidence, we need no overlapping between the CIs. So, we need that the lower bound of the CI of the case without any failed elements is higher than the upper bound of the CI of the case

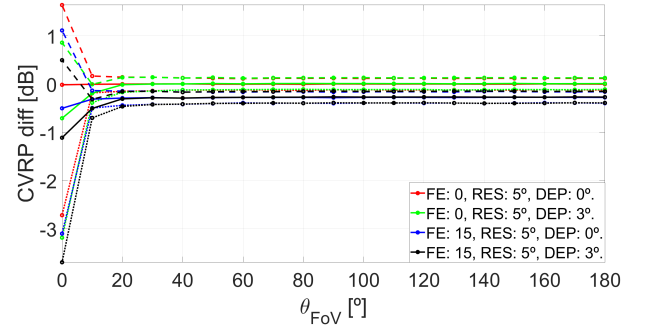


Fig. 5. CVRP difference between the considered cases in the legend and the no faulty element case, with the corresponding angular resolution and without depointing, which we denote as reference. Upper bound of CVRP CI [dBm] minus reference CVRP [dBm] in dashed line. Lower bound of CVRP CI [dBm] minus reference CVRP in dotted line. Average of CVRP with random errors [dBm] minus reference [dBm] in solid line. The considered $\sigma_{err,dB}$ is 1 dB. E.g. the case “FE: 15, RES: 5°, DEP: 3°” is the result of the average of the 1000 CVRP values considering a $\sigma_{err,dB}$ of 1 dB minus the case “FE: 0, RES: 5°, DEP: 0°” without any random error.

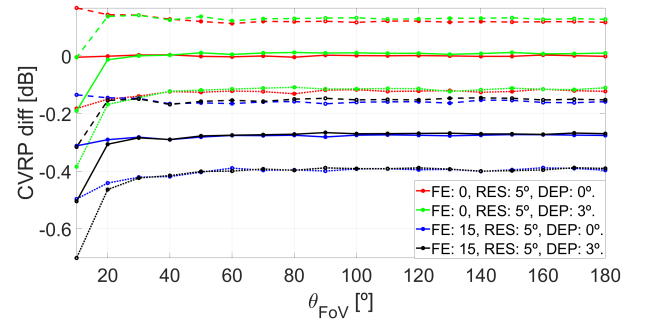


Fig. 6. Zoom of Fig. 5, covering θ_{FoV} from 10° to 180°.

with the failed element. We represent a worst-case scenario in terms of angular resolution and depointing, but not for $\sigma_{err,dB}$. There is a clear overlap for $\theta_{FoV} \leq 30^\circ$, which is rather small for $\theta_{FoV} = 20^\circ$. The same holds for the 45° beamsteered cases. If we check the other failed elements cases, we find out that it is possible to distinguish between them even at $\theta_{FoV} = 10^\circ$ with a 5° angular resolution, as long as $\sigma_{err,dB}$ is kept at 1 dB. This holds for both the broadside and beamsteered cases. It is worth noting that, for most cases, with some exceptions when we compare 0 and 4 failed elements, there are overlaps for the CVRP CIs at $\theta_{FoV} = 0^\circ$. This means that, for the considered error model, $\sigma_{err,dB}$ values and the rest of the factors, it is generally not possible to infer with 95% confidence if there is any failed element only based on the CVRP at $\theta_{FoV} = 0^\circ$. On the other hand, it is also relevant to note that the considered depointing does not represent a noticeable impact on the CVRP values, not making a real difference to be able to distinguish the number of failed elements. Hence, we do not include its effect in the subsequent plots, to avoid excessive clutter. We have checked that the analysis remains virtually the same whether we consider depointing or not. If we make $\sigma_{err,dB} = 2$ dB and we keep the angular resolution at 5° (Fig. 7), then we

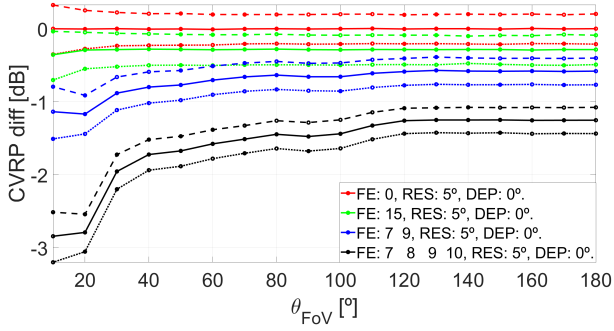


Fig. 7. 45° beamsteering. $\sigma_{err,dB} = 2$ dB. Angular resolution of 5°. All 4 cases of faulty elements are considered. $\theta_{FoV} \in [10^\circ, 180^\circ]$.

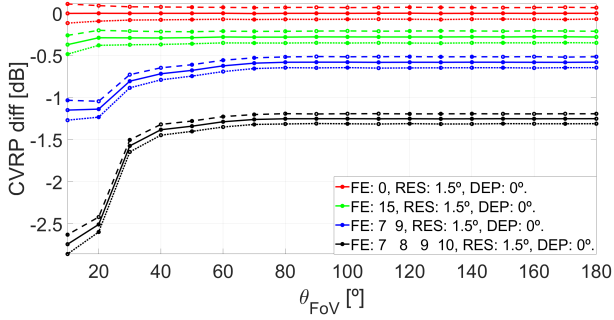


Fig. 8. No beamsteering. $\sigma_{err,dB} = 2$ dB. Angular resolution of 1.5°. All 4 cases of faulty elements are considered. $\theta_{FoV} \in [10^\circ, 180^\circ]$.

see that we are no longer able to reliably distinguish between having 0 or 1 failed elements, or between having 1 or 2 failed elements. It is still possible to reliably distinguish between having 0 or 2 failed elements, as well as between having 0 or 4, 1 or 4, and 2 or 4 failed elements, for any $\theta_{FoV} \geq 10^\circ$. Finally, if we decrease the angular resolution to 1.5°, we can reliably distinguish between all 4 faulty element cases, for any $\theta_{FoV} \geq 10^\circ$.

V. CONCLUSION

In this work, we considered several factors that may impact CVRP values, and their CIs. First, we have shown that the rotation of the pattern in post-processing has a θ_{FoV} -dependent behavior, which can be mitigated by improving the angular resolution (“RES”). In addition, CVRP at $\theta_{FoV} = 0^\circ$ is not useful for determining the presence or number of faulty elements, at least with the error model used. Furthermore, we showed that a 5° angular resolution can distinguish between all four faulty element cases with at least 95% confidence, as long as $\sigma_{err,dB}$ is kept at 1 dB and for $\theta_{FoV} \geq 30^\circ$. For $\sigma_{err,dB} = 2$ dB, improving the angular resolution to 1.5° allows distinction between all four cases for any $\theta_{FoV} \geq 10^\circ$.

These findings imply that CVRP is useful in diagnosing faulty elements within an array, provided the angular resolution is appropriately set. This also depends on the DUT’s behavior when elements fail, as we assume failed elements reduce the TRP proportionally. Importantly, full pattern acquisition is not necessary for diagnosing faulty elements using CVRP, making this method time-efficient. Additionally, since this approach relies only on power values, phase acquisition

is unnecessary unless using a near-field range, which is advantageous for OTA testing. However, this method does not identify specific faulty elements. On the other hand, failures can be identified when the array is calibrated in the factory, but this method aims at diagnosing it at a later stage, without needing full command over the array.

Future work includes using more advanced error models, not considering a proportional decrease of TRP with the failed elements, considering amplitude and (or) phase excitation errors instead of on-off failures, exploring different array topologies, and accounting for variations in TRP output.

ACKNOWLEDGMENT

The work of Alejandro Antón Ruiz is supported by the European Union’s Horizon 2020 Marie Skłodowska-Curie grant agreement No. 955629. Andrés Alayón Glazunov also kindly acknowledges funding from the ELLIIT strategic research environment (<https://elliit.se/>).

REFERENCES

- [1] T. S. Rappaport, S. Sun, R. Mayzus, H. Zhao, Y. Azar, K. Wang, G. N. Wong, J. K. Schulz, M. Samimi, and F. Gutierrez, “Millimeter Wave Mobile Communications for 5G Cellular: It Will Work!” *IEEE Access*, vol. 1, pp. 335–349, 2013.
- [2] P. Zhang, X. Yang, J. Chen, and Y. Huang, “A survey of testing for 5G: Solutions, opportunities, and challenges,” *China Communications*, vol. 16, no. 1, pp. 69–85, 2019.
- [3] O. Breinbjerg and J. Fernandez Alvarez, “Phaseless Near-Field Antenna Measurement Techniques – An Overview,” in *Proceedings of 38th Annual Symposium of the Antenna Measurement Techniques Association*. United States: IEEE, 2016, session 15: General Near-Field Measurement.; 38th Annual Symposium of the Antenna Measurement Techniques Association, AMTA 2016 ; Conference date: 30-10-2016 Through 04-11-2016.
- [4] 5GAA VATM (Vehicular Antenna Test Method). Technical report version 1.0, April 2021.
- [5] A. A. Ruiz, S. Hosseinzadegan, J. Kvarnstrand, K. Arvidsson, and A. A. Glazunov, “Constrained FoV Radiated Power as a Figure of Merit of Phased Arrays,” in *2023 Antenna Measurement Techniques Association Symposium (AMTA)*, 2023, pp. 1–6.
- [6] V. Schenone, A. Fedeli, C. Estatico, M. Pastorino, and A. Randazzo, “Detection of Failures in Antenna Arrays Through a Lebesgue-Space Approach,” *IEEE Open Journal of Antennas and Propagation*, vol. 3, pp. 652–662, 2022.
- [7] G. Oliveri, P. Rocca, and A. Massa, “Failure detection in large arrays through Bayesian compressive sensing,” in *2013 7th European Conference on Antennas and Propagation (EuCAP)*, 2013, pp. 1405–1408.
- [8] C. Xiong and G. Xiao, “A Diagnosing Method for Phased Antenna Array Element Excitation Amplitude and Phase Failures Using Random Binary Matrices,” *IEEE Access*, vol. 8, pp. 33 060–33 071, 2020.
- [9] B.-K. Yeo and Y. Lu, “Fast detection and location of failed array elements using the fast SVM algorithm,” in *2010 14th International Symposium on Antenna Technology and Applied Electromagnetics & the American Electromagnetics Conference*, 2010, pp. 1–4.
- [10] L. de Lange, D. J. Ludick, and T. L. Grobler, “Detecting Failed Elements in an Arbitrary Antenna Array using Machine Learning,” in *2019 International Conference on Electromagnetics in Advanced Applications (ICEAA)*, 2019, pp. 1099–1103.
- [11] M. Ameya and S. Kurokawa, “Element Failure Detection of Array Antenna using Near-field Measurement with Shallow Neural Network,” in *2019 Antenna Measurement Techniques Association Symposium (AMTA)*, 2019, pp. 1–4.
- [12] Mathworks. (2024) Documentation azel2phitheta. [Online]. Available: <https://es.mathworks.com/help/phased/ref/azel2phitheta.html>
- [13] CTIA, “CTIA 01.20 Test Methodology, SISO, Anechoic Chamber. Version 4.0.0,” Feb 2022.
- [14] —, “CTIA 01.70 Measurement Uncertainty. Version 4.0.1,” Nov 2023.
- [15] —, “CTIA 01.73 Supporting Procedures. Version 4.0.4,” Nov 2023.